Rare Met. (2020) 39(11):1256–1261
https://doi.org/10.1007/s12598-020-01468-4

RARE METALS
www.editorialmanager.com/rmet

Enhanced thermoelectric performance of ternary compound Cu_3PSe_4 by defect engineering

Yu-Meng Zhang, Xing-Chen Shen, Yan-Ci Yan, Gui-Wen Wang, Guo-Yu Wang, Jiang-Yu Li, Xu Lu*, Xiao-Yuan Zhou*

Received: 14 February 2020 / Revised: 21 April 2020 / Accepted: 19 May 2020 / Published online: 28 June 2020

Abstract The diamond-like compound Cu_3PSe_4 with low lattice thermal conductivity is deemed to be a promising thermoelectric material, which can directly convert waste heat into electricity or vice versa with no moving parts and greenhouse emissions. However, its performance is limited by its low electrical conductivity. In this study, we report an effective method to enhance thermoelectric performance of Cu_3PSe_4 by defect engineering. It is found that the carrier concentrations of $Cu_{3-x}PSe_4$ (x = 0, 0.03, 0.06, 0.09, 0.12) compounds are increased by two orders of magnitude as $x > 0.03$, from 1×10^{17} to 1×10^{19} cm^{-3}. Combined with the intrinsically low lattice thermal conductivities and enhanced electrical transport performance, a maximum zT value of 0.62 is obtained at 727 K for $x = 0.12$ sample, revealing that Cu defect regulation can be an effective method for enhancing thermoelectric performance of Cu_3PSe_4.

Keywords Cu_3PSe_4; Thermal conductivity; Defect engineering; Electrical conductivity; Thermoelectric performance

Y.-M. Zhang, X.-C. Shen, Y.-C. Yan, X. Lu*, X.-Y. Zhou*
Chongqing Key Laboratory of Soft Condensed Matter Physics and Smart Materials, College of Physics, Chongqing University, Chongqing 401331, China
e-mail: luxu@cqu.edu.cn

X.-Y. Zhou
e-mail: xiaoyuan2013@cqu.edu.cn

X.-C. Shen, G.-Y. Wang
Chongqing Institute of Green and Intelligent Technology, Chinese Academy of Science, Chongqing 400714, China

X.-C. Shen, G.-Y. Wang
University of Chinese Academy of Sciences, Beijing 100044, China

G.-W. Wang, X.-Y. Zhou
Analytical and Testing Center of Chongqing University, Chongqing 401331, China

J.-Y. Li
Shenzhen Key Laboratory of Nanobiomechanics, Shenzhen Institutes of Advanced Technology, Chinese Academy of Sciences, Shenzhen 518055, China

1 Introduction

Thermoelectric (TE) materials can directly convert waste heat into electricity or vice versa with no moving parts and greenhouse emissions [1–4], which offers an alternative strategy to solve the growing serious energy and environment issues as a complement to other renewable energy resources. The performance of TE materials is defined by the thermoelectric figure of merit $zT = \sigma S^2 T\ (\kappa_e + \kappa_L)^{-1}$, where σ is the electrical conductivity, S is the Seebeck coefficient, κ_e is the electronic thermal conductivity, κ_L is the lattice thermal conductivity and T is the absolute temperature [5]. Many efforts have been made to improve the thermoelectric performance by manipulating the electrical transport or phonon transport properties [6–8]. However, the electrical conductivity, Seebeck coefficient and electronic thermal conductivity are physically intertwined, which sets obstacle for the continuous enhancement of zT. Fortunately, the lattice thermal conductivity is the relatively independent parameter among above transport parameters. Therefore, it is feasible to discover some novel TE compounds with intrinsically low thermal conductivity where we can start to tune the electrical transport properties through regulating carrier concentration,

scattering mechanisms or band degeneracy, such as the accomplishment in SnSe, Mg_3Sb_2 and BiCuSeO [9–14]. Recent studies have shown that the complex derivative compounds with a series of primitive cells based on Groups II–VI such as ternary I–III–VI_2, II–IV–V_2, II–III_2–VI_4, I_2–IV–VI_3, I_3–V–VI_4 and quaternary I_2–II–IV–VI_4 compounds can be synthesized [15–19]. Compared with binary compounds, the numbers of atoms in ternary or quaternary compounds increase, and consequently, the contribution from the acoustic phonons, which are mainly responsible for heat transport, decreases to the overall heat capacity. As a result, the lattice thermal conductivity decreases drastically. On the other hand, these multi-component derivatives enrich the range of constituent elements, providing more selectable doping elements to effectively improve electrical properties. Therefore, a ternary or quaternary compound with a diamond-like structure is expected to be a potential thermoelectric material. However, researchers are currently less concerned about the I_3–V–VI_4 alloys except for Cu_3SbSe_4-based compounds. According to different compositional elements, there are two types of crystal structures for these compounds, in which one is tetragonal structure, such as Cu_3SbSe_4, and the other is orthorhombic structure, like Cu_3PSe_4. In 2016, the thermoelectric properties of pure Cu_3PSe_4 were preliminarily studied, which exhibits a lattice thermal conductivity lower than several typical Cu-based TE compounds at room temperature, including Cu_3SbSe_4, $CuInTe_2$ and $CuFeS_2$ [20–22]. However, the low carrier concentration of the pure sample results in poor electrical performance and the large band gap of the Cu_3PSe_4 makes it difficult to enlarge the carrier concentration by conventional substitutional doping [23].

In this work, an alternative approach involving defect engineering is purposed to promote power factor (PF) by introducing Cu vacancy in wide band gap diamond-like Cu_3PSe_4 compound, which has been performed on other TE compounds. All deficiency samples show increased carrier concentration and improved electrical properties while maintain the low lattice thermal conductivities.

2 Experimental

2.1 Sample preparation

Polycrystalline $Cu_{3-x}PSe_4$ (x = 0, 0.03, 0.06, 0.09, 0.12) samples were synthesized by traditional solid-state reaction method combined with spark plasma sintering (SPS). Stoichiometric amounts of elemental Cu, P and Se with 99.99% purity were weighed and mixed as starting materials. Then, they were sealed in vacuum quartz tubes ($\sim 1\times10^{-4}$ Pa) and slowly heated to 723 K at a speed of 2 K·min^{-1}, kept at this temperature for 20 h and then cooled down to room temperature naturally. The ingots were ground into fine powders and then consolidated by pressing at room temperature. The products were annealed at 723 K for another 20 h. Finally, the powers were consolidated into cylinder samples with 10 mm diameters by SPS at 723 K for 5 min under a pressure of 75 MPa. The final products were confirmed to reach 97% of the theoretical density.

2.2 Sample characterization

The phase purity of all samples was checked through powder X-ray diffraction (XRD) on a PANalytical X'Pert apparatus with Cu Kα radiation (40 kV, 40 mA, λ = 0.15406 nm). Transmission electron microscopy (TEM) characterizations were performed on a probe-corrected FEI Titan G2 microscope. The electrical conductivity (σ) and Seebeck coefficient (S) were measured by a Linseis LSR-3 system under the protection of helium, and the thermal conductivity (κ) was calculated from formula $\kappa = \rho C_p D$, where thermal diffusivity (D) was obtained by laser flash technique microflash LFA system (NETZSCH, LFA 457), density (ρ) was measured by the Archimedes method, and the specific heat (C_p) was estimated using Dulong–Petit value. The measurement errors were about 5%, 5% and 3% for electrical conductivity, Seebeck coefficient and thermal conductivity, respectively. The room-temperature carrier concentrations were measured by a homemade Hall apparatus under a magnetic field of ± 1 T.

3 Results and discussion

Figure 1a shows the room-temperature crystal structures of Cu_3PSe_4. The Wurtzite-derived diamond-like compound Cu_3PSe_4 crystallizes in orthorhombic structure, belonging to space group $Pmn2_1$ with lattice parameters of a = 0.7685 nm, b = 0.6656 nm, c = 0.6377 nm, Z = 2. The three-dimensional structure shown in Fig. 1a can be considered as a stacking of [Cu (2) Se_4] tetrahedron layer and [Cu (1)–P–Se] tetrahedron layer along the b-direction [24, 25]. From the crystallographic information of Cu_3PSe_4, there are two non-equivalent crystallographic positions of Cu atoms in lattice, which will be used to confirm our low-temperature heat capacity fitting result. The room-temperature XRD patterns for $Cu_{3-x}PSe_4$ (x = 0, 0.03, 0.06, 0.09, 0.12) are shown in Fig. 1b. All peaks can be indexed to the standard reference PDF No.78-575, indicating that all of the samples are single phased within the limitation dictation of apparatus. Figure 1c shows the refined lattice parameters of the unit cell of $Cu_{3-x}PSe_4$ (x = 0, 0.03, 0.06, 0.09, 0.12) obtained from MDI Jade 6

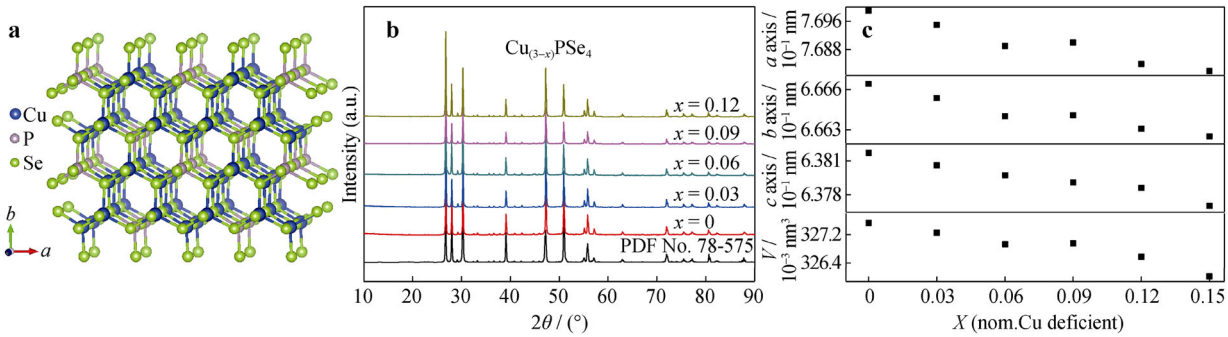

Fig. 1 **a** Crystal structure of Cu_3PSe_4; **b** XRD patterns of $Cu_{3-x}PSe_4$ (x = 0, 0.03, 0.06, 0.09, 0.12); **c** lattice parameters of unit cell of $Cu_{3-x}PSe_4$ (x = 0, 0.03, 0.06, 0.09, 0.12) via Rietveld refinement

software. The lattice constant is decreasing with increasing Cu vacancy, consistent with our expectation that Cu vacancy will lead to shrink of lattice.

The images of energy-dispersive spectroscopy (EDS) elemental mapping, shown in Fig. 2, indicate the uniform element distribution throughout the sample. Figure 3a shows the total thermal conductivity as a function of temperature for $Cu_{3-x}PSe_4$ (x =0, 0.03, 0.06, 0.09, 0.12) compounds. It is found that the total thermal conductivities of all compounds are decreasing with increasing temperature over the entire temperature range. Interestingly, the thermal conductivity of different samples shows a contrary dependence on Cu vacancy content. For example, the total thermal conductivity of Cu_3PSe_4 is only 1.37 $W{\cdot}m^{-1}{\cdot}K^{-1}$ while the value of $Cu_{2.88}PSe_4$ is as high as 1.62 $W{\cdot}m^{-1}{\cdot}K^{-1}$. The electronic thermal conductivity, which is shown in Fig. 3b, is estimated by $\kappa_e = L\sigma T$, where L is the Lorenz number calculated from the single parabolic band model, assuming ionized impurity scattering or acoustic phonon scattering dominates. Then, by subtracting the electronic thermal conductivities from the total thermal conductivities, the lattice thermal conductivities of sample are attained and shown in Fig. 3c. The lattice thermal conductivity shows approximately the same trend and value as total thermal conductivity, which implies the total thermal conductivities of all samples are almost dominated by lattice contribution over the entire temperature range. Furthermore, the room-temperature lattice thermal conductivity of Cu_3PSe_4 is 1.37 $W{\cdot}m^{-1}{\cdot}K^{-1}$, which is lower than those of other Cu-based compounds like Cu_3SbSe_4 (2.91 $W{\cdot}m^{-1}{\cdot}K^{-1}$) [26], $CuInTe_2$ (5.40 $W{\cdot}m^{-1}{\cdot}K^{-1}$) [17] and $CuFSe_2$ (5.90 $W{\cdot}m^{-1}{\cdot}K^{-1}$) [27]. In order to probe the details about the underlying lattice dynamics of low lattice thermal conductivity of Cu_3PSe_4, the low-temperature heat capacity (C_p) of Cu_3PSe_4 was measured and can be well fitted with the Debye lattice mode and two Einstein oscillators, as shown in Fig. 3d. The fitting is performed based on the following equation

$$\frac{C_p}{T} = \beta T^2 + A(\Theta_{E1})^2 T^3 \frac{e^{\Theta_{E1}/T}}{(e^{\Theta_{E1}/T} - 1)^2} + B(\Theta_{E2})^2 T^3 \frac{e^{\Theta_{E2}/T}}{(e^{\Theta_{E2}/T} - 1)^2} \quad (1)$$

where βT^2 term is the Debye term based on long wavelength acoustic modes, A and B are constants, while Θ_{E1} and Θ_{E2} are the characteristic temperatures of two Einstein modes. The best fitting parameters are β = 0.11 $mJ{\cdot}mol^{-4}$, A = 0.40 $J{\cdot}mol^{-1}{\cdot}K^{-1}$, B = 2.50 $J{\cdot}mol^{-1}{\cdot}K^{-1}$, Θ_{E1} = 58 K, Θ_{E2} = 65 K. The fitting parameters $A + B$ = 2.9 are closed to 3, which is the number of Cu atoms per molecular formula. Besides, two Einstein modes are associated with the two different local vibrational modes resulting from two types of Cu atoms [28, 29]. From the discussion above, we speculate that the local vibration of Cu atoms plays a vital role in the observed intrinsically low lattice thermal

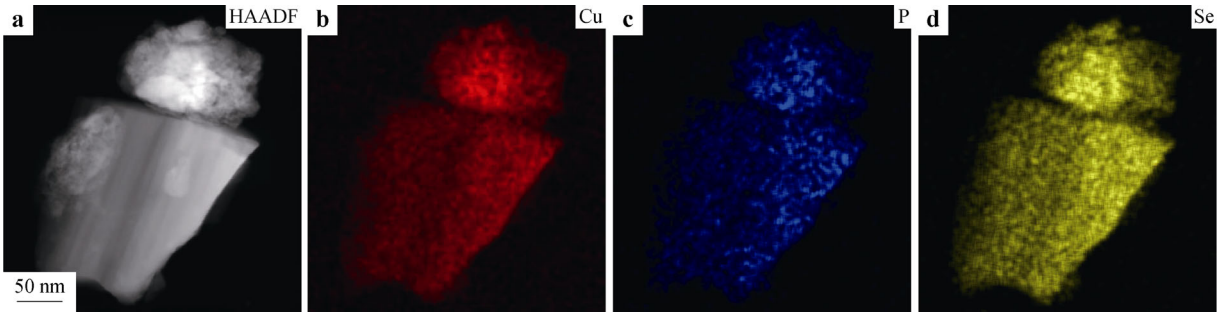

Fig. 2 **a** High-angle annular dark field (HAADF) image; elemental mappings for **b** Cu (red), **c** P (blue) and **d** Se (yellow)

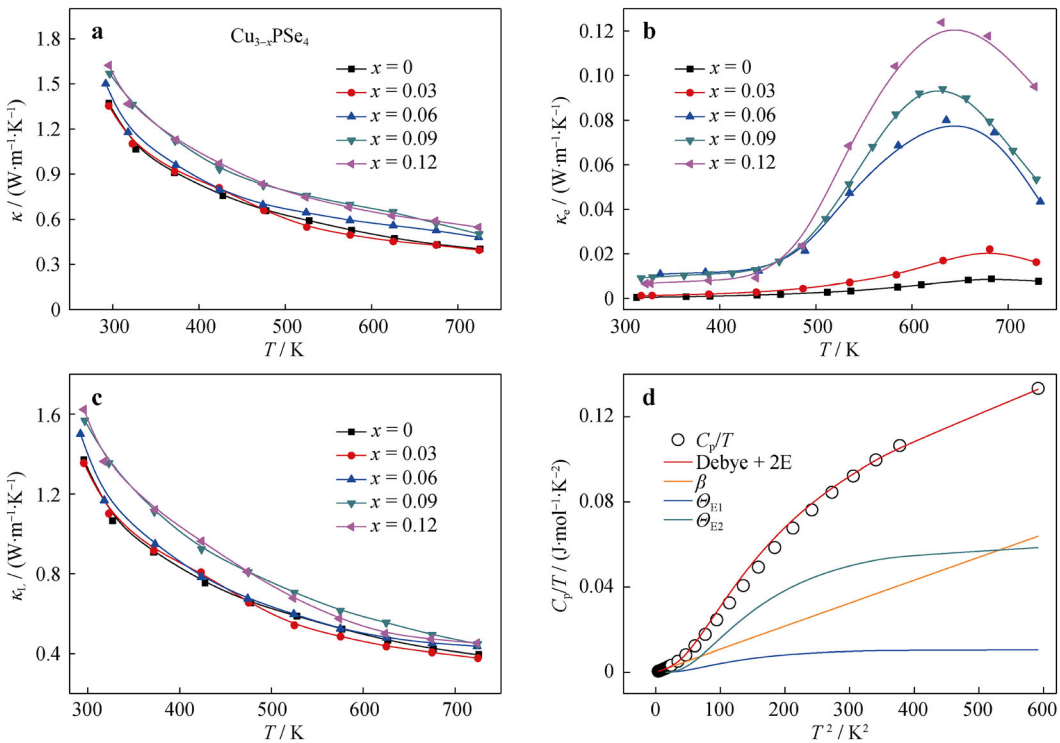

Fig. 3 Thermal transport properties of $Cu_{3-x}PSe_4$ (x =0, 0.03, 0.06, 0.09, 0.12) compounds as a function of temperature: **a** total thermal conductivity; **b** electronic thermal conductivity; **c** lattice thermal conductivity and **d** C_p/T vs. T^2 for Cu_3PSe_4 (black circles), where red solid line shows fitted curve by using a Debye lattice plus two Einstein modes, and other colored lines are Debye term β and two Einstein temperatures (Θ_{E1} and Θ_{E2})

conductivity of these compounds, which means the reduction in Cu content potentially weakens such effect. Therefore, the variation in lattice thermal conductivity should depend on the competition between Cu-induced anharmonicity and vacancy scattering. Thus, the observed increase in lattice thermal conductivity with x increasing is reasonable, assuming the latter mechanism dominates at room temperature. The same phenomenon was observed in $Cu_{12}Sb_4S_{13}$ compounds when Sb, which contributes to the low lattice thermal conductivity, was replaced by other elements.

Figure 4 presents electrical transport properties of $Cu_{3-x}PSe_4$ (x = 0, 0.03, 0.06, 0.09, 0.12) samples. As shown in Fig. 4a, the pristine Cu_3PSe_4 presents relatively low electrical conductivity at room temperature which is attributed to the low carrier concentration of the pristine compound. It is clear to see that the room-temperature electrical conductivity of $Cu_{3-x}PSe_4$ firstly increases with Cu vacancy increasing ($x \leq 0.06$), and then decreases ($x > 0.06$), which results from the competition between the carrier concentration and the mobility as listed in Table 1. What is more, it can be seen from the table that the room-temperature carrier concentration increases dramatically with vacancy content increasing, which successfully boosts the carrier concentration from 1×10^{17} to 1×10^{19} cm^{-3}, making the $Cu_{2.94}PSe_4$ sample most conducting sample with electrical conductivity value of 1648 S m^{-1} at room temperature among Cu-deficient compounds. As the temperature increases, such competition mechanism continues to work. All samples show a trend of electrical conductivity increasing firstly and then decreasing with increasing temperature. Finally, the electrical conductivity of $Cu_{2.88}PSe_4$ reaches a maximum value of 8009 S m^{-1}, around 630 K. The temperature-dependent Seebeck coefficient for $Cu_{3-x}PSe_4$ is depicted in Fig. 4b, and all samples show the positive values, implying that the major carriers are holes. With temperature increasing, the Seebeck coefficients of the pristine and lightly deficient samples drop while that for the samples with more Cu vacancy show slightly increase with respect to temperature. To fully comprehend the electrical transport behavior, the temperature-dependent carrier concentration and mobility have been measured. As shown in Fig. 4c, the carrier concentration of samples with small Cu vacancy content ($x < 0.06$) shows a strong temperature dependence, suggesting the non-degenerate semiconductor behavior of these samples. With the increase in Cu vacancy content, it is expected that the carriers donated by the defect level are ionized near room-temperature region, and the carrier concentration is greatly increasing to the order of

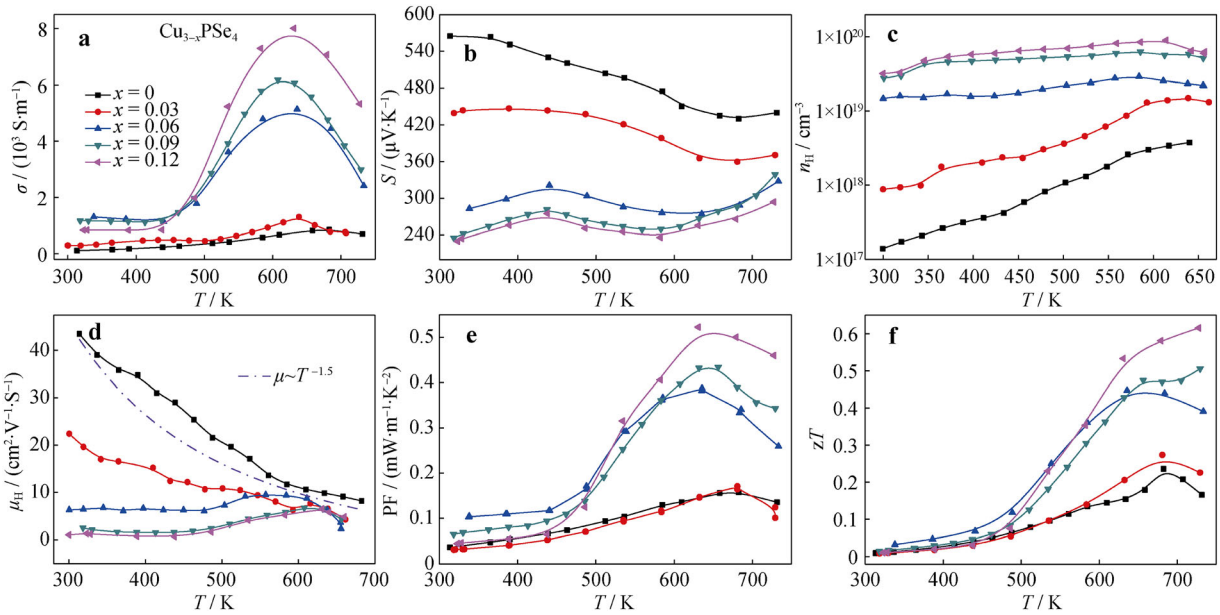

Fig. 4 Electrical transport properties of $Cu_{3-x}PSe_4$ (x = 0, 0.03, 0.06, 0.09, 0.12) solid solutions: **a** temperature-dependent electrical conductivity; **b** temperature-dependent Seebeck coefficient; **c** temperature-dependent carrier concentration; **d** temperature-dependent carrier mobility; **e** power factor; and **f** zT values

Table 1 Relationship of electrical properties of material with doping amount at room temperature

Compositions	n_H/(10^{18} cm^{-3})	μ/(cm^2·V^{-1}·S^{-1})	σ/(S·m^{-1})	S/(μV·K^{-1})	PF/(mW·m^{-1}·K^{-2})
Cu_3PSe_4	0.139	51.26	114	564.8	0.036
$Cu_{2.97}PSe_4$	0.877	21.09	296	439.3	0.032
$Cu_{2.94}PSe_4$	14.800	6.96	1304	283.0	0.104
$Cu_{2.91}PSe_4$	27.800	2.63	1170	235.3	0.065
$Cu_{2.88}PSe_4$	29.000	1.81	839	229.8	0.044

10^{19} cm^{-3}. In Fig. 4d, when $x < 0.06$, the mobility of all Cu-deficient samples follows a $T^{-1.5}$ linear behavior, indicating the acoustic phonon scattering plays a dominant role in these compounds. As the vacancy content increases, the mobility decreases rapidly near room temperature, which may be due to the ionized impurity scattering. The mobility of samples with high concentration of Cu vacancy shows relative temperature independent behavior, which suggests the domination of ionized impurity scattering [30]. Benefiting from the largely enhanced electrical conductivity and the moderately diminished Seebeck coefficients, the highest power factor of 0.55 mW·m^{-1}·K^{-2} at 630 K is obtained for the sample $Cu_{2.88}PSe_4$ (Fig. 4e). Furthermore, as a result of the enhancement in electrical transport performance and the intrinsically low thermal conductivity, the thermoelectric performance of Cu_3PSe_4 has been considerably improved. Ultimately, a maximum zT value of 0.62 is attained at 727 K for x = 0.12 sample, which is almost three times enhancement compared to the pristine sample (Fig. 4f). From the above analysis, it can be seen that the defect engineering in Cu_3PSe_4 can effectively improve the electrical transport properties while maintain relatively low thermal conductivity.

4 Conclusion

In summary, the p-type $Cu_{3-x}PSe_4$ (x =0, 0.03, 0.06, 0.09, 0.12) compounds with diamond-like structure have been successfully synthesized by solid melting reaction. The maximum zT value of 0.62 at 727 K is achieved in $Cu_{2.88}PSe_4$ by rational defect engineering. By regulating the Cu vacancy content in pristine sample, we successfully boost the carrier concentration from 1×10^{17} to 1×10^{19} cm^{-3} while maintaining the low lattice thermal conductivity of all deficient samples. Thereby, the large enhancement in electrical conductivity and thermoelectric performance are attained. This work reveals that Cu defect

regulation can be an effective method for enhancing thermoelectric performance of Cu_3PSe_4, which will shed light on the strategy for promoting the thermoelectric performance of other wide band gap compounds with similar structure.

Acknowledgements This work was financially supported by the Graduate Scientific Research and Innovation Foundation of Chongqing, China (No. CYB 19064), the Project for Fundamental and Frontier Research in Chongqing (No. CSTC2017JCYJAX0388), Shenzhen Science and Technology Innovation Committee (No. JCYJ20170818155752559), the National Natural Science Foundation of China (Nos. 51772035, 11674040 and 51472036) and the Fundamental Research Funds for the Central Universities (No. 106112017CDJQJ308821). We would like to thank the Analytical and Testing Center of Chongqing University for the assistance with the Hall measurements.

References

[1] Zhou X, Yan Y, Lu X, Zhu H, Han X, Chen G, Ren Z. Routes for high-performance thermoelectric materials. Mater Today. 2018;21(9):974.
[2] Bell LE. Cooling, heating, generating power, and recovering waste heat with thermoelectric systems. Science. 2008; 321(5895):1457.
[3] Goldsmid HJ, Nolas GS. In A Review of the New Thermoelectric Materials, Ict 20 International Conference on Thermoelectrics, Beijing. 2001. 1.
[4] Snyder GJ, Toberer ES. Complex thermoelectric materials. Nat Mater. 2008;7(2):105.
[5] Tritt TM, Subramanian MA. Thermoelectric materials, phenomena, and applications: a bird's eye view. MRS Bull. 2011; 31(3):188.
[6] Peng K, Zhang B, Wu H, Cao X, Li A, Yang D, Lu X, Wang G, Han X, Uher C. Ultra-high average figure of merit in synergistic band engineered $Sn_xNa_{1-x}Se_{0.9}S_{0.1}$ single crystals. Mater Today. 2018;21(5):501.
[7] Zhang SS, Yang DF, Shaheen N, Shen XC, Xie DD, Yan YC, Lu X, Zhou XY. Enhanced thermoelectric performance of CoSb $S_{0.85}Se_{0.15}$ by point defect. Rare Met. 2018;37(4):326.
[8] Chen Z, Zhang X, Pei Y. Manipulation of phonon transport in thermoelectrics. Adv Mater. 2018;30(17):e1705617.
[9] Zhao LD, Lo SH, Zhang Y, Sun H, Tan G, Uher C, Wolverton C, Dravid VP, Kanatzidis MG. Ultralow thermal conductivity and high thermoelectric figure of merit in SnSe crystals. Nature. 2014;508(7496):373.
[10] Mao J, Shuai J, Song S, Wu Y, Dally R, Zhou J, Liu Z, Sun J, Zhang Q, Dela Cruz C. Manipulation of ionized impurity scattering for achieving high thermoelectric performance in n-type Mg3Sb2-based materials. Proc Natl Acad Sci. 2017;114(40): 10548.
[11] Li Z, Xiao C, Fan S, Deng Y, Zhang W, Ye B, Xie Y. Dual vacancies: an effective strategy realizing synergistic optimization of thermoelectric property in BiCuSeO. J Am Chem Soc. 2015;137(20):6587.
[12] Yao Z, Li W, Tang J, Chen Z, Lin S, Biswas K, Burkov A, Pei Y. Solute manipulation enabled band and defect engineering for thermoelectric enhancements of SnTe. InfoMat. 2019;1(4):571.
[13] Tang J, Yao Z, Chen Z, Lin S, Zhang X, Xiong F, Li W, Chen Y, Pei Y. Maximization of transporting bands for high-performance SnTe alloy thermoelectrics. Mater Today Phys. 2019;9:100091.
[14] Wang X, Li W, Zhou B, Sun C, Zheng L, Tang J, Shi X, Pei Y. Experimental revelation of multiband transport in heavily doped $BaCd_2Sb_2$ with promising thermoelectric performance. Mater Today Phys. 2019;8:123.
[15] Shi X, Xi L, Fan J, Zhang W, Chen L. Cu–Se bond network and thermoelectric compounds with complex diamondlike structure. Chem Mater. 2010;22(22):6029.
[16] Zhang A, Chen Q, Yao W, Yang D, Wang G, Zhou X. Large-scale colloidal synthesis of co-doped Cu_2SnSe_3 nanocrystals for thermoelectric applications. J Electron Mater. 2016;45(3): 1935.
[17] Liu R, Xi L, Liu H, Shi X, Zhang W, Chen L. Ternary compound $CuInTe_2$: a promising thermoelectric material with diamond-like structure. Chem Commun. 2012;48(32):3818.
[18] Cho J, Shi X, Salvador JR, Meisner GP, Yang J, Wang H, Wereszczak AA, Zhou X, Uher C. Thermoelectric properties and investigations of low thermal conductivity in Ga-doped Cu_2GeSe_3. Phys RevB. 2011;84(8):085207.
[19] Zhang H, Li JT, Ding FZ, Qu F, Li H, Gu HW. Combustion synthesis of ZrNiSn half-Heusler thermoelectric materials%. Chin J Rare Met. 2019;043(4):337.
[20] Qiu W, Wu L, Ke X, Yang J, Zhang W. Diverse lattice dynamics in ternary Cu–Sb–Se compounds. Sci Rep. 2015;5:13643.
[21] Wang G, Yu D, Guo L, Yang D, Hu C, Peng K, Zhang Q, Tang X, Wang G, Zhou X. Rapid fabrication of $CuInSb_xTe_{2-x}$ ($0 \le x \le 0.10$) compounds and their thermoelectric performance. Sci Adv Mater. 2015;7(12):2672.
[22] Qiu P, Shi X, Chen L. Cu-based thermoelectric materials. Energy Storage Mater. 2016;3:85.
[23] Foster D, Jieratum V, Kykyneshi R, Keszler D, Schneider G. Electronic and optical properties of potential solar absorber Cu_3PSe_4. Appl Phys Lett. 2011;99(18):181903.
[24] Foster D, Barras F, Vielma J, Schneider G. Defect physics and electronic properties of Cu_3PSe_4 from first principles. Phys Rev B. 2013;88(19):195201.
[25] Pfitzner A, Reiser S. Refinement of the crystal structures of Cu_3PS_4 and Cu_3SbS_4 and a comment on normal tetrahedral structures. Z für Kristallographie-Cryst Mater. 2002;217(2):51.
[26] Skoug EJ, Cain JD, Morelli DT, Kirkham M, Majsztrik P, Lara-Curzio E. Lattice thermal conductivity of the Cu_3SbSe_4-Cu_3SbS_4 solid solution. J Appl Phys. 2011;110(2):023501.
[27] Li Y, Zhang T, Qin Y, Day T, Jeffrey Snyder G, Shi X, Chen L. Thermoelectric transport properties of diamond-like $Cu_{1-x}Fe_{1+x}S_2$ tetrahedral compounds. J Appl Phys. 2014;116(20): 203705.
[28] Shen X, Yang CC, Liu Y, Wang G, Tan H, Tung YH, Wang G, Lu X, He J, Zhou X. High-temperature structural and thermoelectric study of argyrodite Ag_8GeSe_6. ACS Appl Mater Interfaces. 2018;11(2):2168.
[29] Shen X, Xia Y, Wang G, Zhou F, Ozolins V, Lu X, Wang G, Zhou X. High thermoelectric performance in complex phosphides enabled by stereochemically active lone pair electrons. J Mater Chem A. 2018;6(48):24877.
[30] Shuai J, Mao J, Song S, Zhu Q, Sun J, Wang Y, He R, Zhou J, Chen G, Singh DJ, Ren Z. Tuning the carrier scattering mechanism to effectively improve the thermoelectric properties. Energy Environ Sci. 2017;10(3):799.